Simulation of tomosynthesis images based on an anthropomorphic software breast tissue phantom

Nicole V. Ruiter[a,b], Cuiping Zhang[a,c], Predrag R. Bakic[a], Ann-Katherine Carton[a], Johnny Kuo[a] and Andrew D.A. Maidment[a]

[a]University of Pennsylvania, Philadelphia, PA, USA;
[b]Forschungszentrum Karlsruhe, Karlsruhe, Germany;
[c]Delaware State University, Dover, DE, USA

ABSTRACT

The aim of this work is to provide a simulation framework for generation of synthetic tomosynthesis images to be used for evaluation of future developments in the field of tomosynthesis. An anthropomorphic software tissue phantom was previously used in a number of applications for evaluation of acquisition modalities and image post-processing algorithms for mammograms. This software phantom has been extended for similar use with tomosynthesis. The new features of the simulation framework include a finite element deformation model to obtain realistic mammographic deformation and projection simulation for a variety of tomosynthesis geometries. The resulting projections are provided in DICOM format to be applicable for clinically applied reconstruction algorithms. Examples of simulations using parameters of a currently applied clinical setup are presented. The overall simulation model is generic, allowing multiple degrees of freedom to cover anatomical variety in the amount of glandular tissue, degrees of compression, material models for breast tissues, and tomosynthesis geometries.

Keywords: Modeling, Validation, Diagnosis

1. INTRODUCTION

Tomosynthesis is an emerging imaging modality currently under investigation for breast cancer screening. Several low-dose mammograms are acquired at different x-ray tube angles and used to reconstruct a 3D image of the breast. Recent studies have shown that 3D imaging with tomosynthesis is superior to mammography in sensitivity and specificity for breast cancer detection and thus might overcome the problem of superimposed tissue structures, one of the main disadvantages of mammography.[1,2]

In this paper we describe a simulation framework for generation of synthetic tomosynthesis projections and volumes. The simulation is based on the use of an anthropomorphic software breast tissue phantom, previously developed for generation of synthetic mammograms.[3] Software phantoms provide known ground truth and flexibility in simulation of the breast anatomy. Applications of such simulated images include optimization of image acquisition modalities and evaluation of image post-processing algorithms. The anthropomorphic breast phantom has been used previously for evaluation of mammogram registration methods,[4] estimation of tissue specific radiation dose in mammography,[5] and design of radiation treatment protocols.[6]

In this work, we extend the existing simulation framework by introducing a finite element model capable of realistic simulation of mammographic deformation.[7] The resulting deformed software phantoms are subsequently used for simulation of phantom tomosynthesis projections. Reconstructed tomosynthesis volumes are obtained using clinical reconstruction algorithms. We describe and illustrate the methods for finite elements deformation modeling and tomosynthesis projection simulation.

Further author information: N.V. Ruiter: E-mail: ruiter@ipe.fzk.de, telephone: (+49) 7247 82 5668. Address: Institute for Data Processing and Electronics, Forschungszentrum Karlsruhe, Hermann–von–Helmholtz–Platz 1, 76344 Eggenstein–Leopoldshafen, Germany
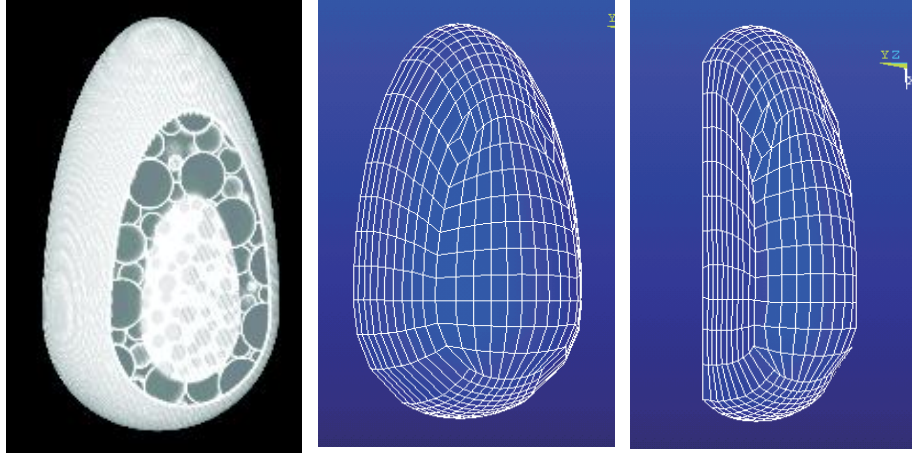
Figure 1. Example of an uncompressed anthropomorphic breast phantom (left) and its FEM model (center). The right figure shows the FEM model after compressing the breast phantom; the compression results in a 50 % reduced breast thickness.

2. ANTHROPOMORPHIC SOFTWARE BREAST TISSUE PHANTOM

An anthropomorphic software breast phantom has been designed previously[3] as a generic 3D model of the breast anatomy. Phantom elements are simulated in the form of geometric primitives, based upon the size and distribution of large and medium scale breast tissue structures. It has been shown that the texture properties of the resulting synthetic mammograms are comparable with clinical mammograms.[8]

The phantom consists of a simulated breast outline formed by quarters of two ellipsoids and are covered by a thin layer simulating skin. In the interior, a region of predominantly adipose tissue (AT) surrounds a central, ellipsoidally shaped region of predominantly fibroglandular tissue (FGT). The Cooper's ligaments in the AT region are modeled as a honeycomb structure. The compartments of the structure are modeled as thin connected shells surrounding the fatty tissue. In the FGT region small compartments of adipose tissue are enclosed in the glandular tissue. The number and the size of the adipose compartments can be parameterized to simulate variation in breast volumes, glandularity, and mammographic texture. A 3D region growing algorithm is applied to simulate compartments of different sizes and orientations. An example model is shown in Fig. 1. More details about the phantom are decribed by Zhang, et al.[9]

3. FINITE ELEMENT MODEL OF MAMMOGRAPHIC BREAST DEFORMATION

The anthropomorphic breast phantom models an undeformed breast. During mammography and tomosynthesis examinations the breast is deformed significantly to reduce radiation dose and to improve image quality. The compression is applied by squeezing the breast between two plexiglas plates in the direction of the projection. The compression causes a decrease in thickness of the breast of approximately 20 to 50 % and thus applies a significant non-linear deformation to the soft breast tissue. Hence a realistic simulation of the mammographic compression is necessary for realistic simulation of tomosynthesis images.

3.1 State of the art of deformation models for the breast

Several deformation models for mammographic compression have been proposed in the literature. The most advanced models are based on the finite element method (FEM), simulating the physical behavior of the breast.[7, 10–13] All of these models use patient images directly to generate the FEM model, so that the model is patient specific. They differ in the applied material models for the tissues and the formulation of the breast compression.

The deformation model applied here is based on the finite element model proposed by Ruiter et al.[7] It has been developed previously for registration of mammograms and breast MR images. It features different

non-linear material models. Additionally, the deformation of the model can be directly defined as deformation by the compression plates, only requiring the percentage of the desired compression as an input parameter. An example for such a model is shown in Fig. 1.

3.2 Finite element method for breast deformation

FEM [14] is a method for numerical solution of a physical problem described in a variational formulation. For problems of solid mechanics the deformation state of a body can be approximated by means of the total potential energy. The basic idea of FEM is to divide the deformable body into finite elements, which are joined at discrete nodes. To ensure the continuity within the body, aligning constraints are introduced at the connecting nodes. The system is discretized by representing the desired function (displacement, strain or stress) within each element as a (finite) sum of element specific interpolation functions, the so–called shape functions.

The equilibrium equations for small deformations based on the total potential energy for a linear elastic body can be derived by a linear approximation of the total potential energy Π. Then the problem may be described by the displacement vector $\{u\}$ of each point within the deformed body $\mathcal{B}$, where $\{\varepsilon\}$ is the vector formulation of the Cauchy strain tensor:[15]

$$\Pi(\{u\}) = \sum_{e=1}^{L} \left[\int_{\mathcal{B}_e} \frac{1}{2}\{\varepsilon\}^T[D]\{\varepsilon\}dv - \int_{\mathcal{B}_e} \{f\}^T\{u\}dv - \int_{\mathcal{S}_{\mathcal{B}_e}} \{t\}^T\{u\}ds \right]. \tag{1}$$

The first term on the right hand side is the total internal elastic strain energy, and the second and third term are the potential energy of the external volumetric and surface loads, in each case for one finite element $\mathcal{B}_e$, with $e = 1, ..., L$. The volume of an element $\mathcal{B}_e$ is denoted as dv and the surface of an element $\mathcal{S}_{\mathcal{B}_e}$ as ds. The vector formulation $\{\sigma\}$ of the stress tensor is expressed by the generalized Hook's law as $\{\sigma\} = [D]\{\varepsilon\}$. $[D]$ is a linear matrix, relating stress and strain components for a linear elastic system. $\{f\}$ are the body forces and $\{t\}$ the surface tractions. After minimization of the total potential energy of the body the desired entity like displacement or stress can be calculated at arbitrary points.

The derivation above assumes small deformations of linear elastic materials. To model the significant mammographic deformation, geometric non-linearities have to be taken into account. The Π of a body subjected to large deformation in respect to the current configuration $\mathcal{C}^t$ can then be written as:

$$\Pi = \int_{\mathcal{B}^{\mathcal{C}^t}} \{\varepsilon\}^T\{\sigma\}dv - \int_{\mathcal{B}^{\mathcal{C}^t}} \{f\}^T\{u\}dv - \int_{\mathcal{S}_{\mathcal{B}}^{\mathcal{C}^t}} \{t\}^T\{u\}ds. \tag{2}$$

Small-step incremental solution methods are used to solve non-linear FE equation systems; for example, the Newton-Raphson method. In the simplified incremental solution process the loads applied to the body are formulated by a set of incremental loads, so that changes in the loads and material properties due to finite strains can be modeled by $e.g.$ $\triangle\{f\}^i$, where $\{f\}^{n+1} = \{f\}^n + \triangle\{f\}^{n+1}$. Starting with the body in the reference configuration, the $(n+1)^{th}$ solution vector $\{u\}^{(n+1)}$ is calculated using the updated values. Then non-linear material models can also be considered, where the stress-strain relationship is dependent on the actual strain rate.

We employed the commercial finite elements software Abaqus (Simulia, Providence, R.I., USA, Version 6.6) to formulate and solve the FEM problem.

3.3 Meshing algorithm

The finite element models used for medical purposes are often based on patient images. This has the advantage that the shape and composition of the model is highly realistic and that the model is specific for a patient. The generation of the geometry of the model, the finite element mesh, is then done based on segmented images, rather than on CAD (computer aided design) models or on geometric primitives, a common method to generate a FEM model. Generating a model from images poses a challenge mainly as it is important for finite element meshes to have continuous boundaries and to consist of as few finite elements as possible. But digital images contain many stairstep-shaped boundaries and are usually converted to many finite elements. There are many different

approaches for generation of finite element meshes which try to solve that problem with different emphases. Currently, there is no commonly accepted approach.

For this application the geometry of the finite element mesh is generated based on a 3D image of the software phantom and a look-up table mapping the different breast tissues to the gray values of the phantom. An unstructured meshing method for tetrahedral finite elements was chosen to enable a denser mesh at tissue borders and a coarser mesh in homogenous regions. We based the meshing on Distmesh,[16] which applies the following steps:

1. generate a regular mesh of nodes covering a rectangular volume including the object to be meshed and discard all nodes outside the object,

2. reduce the number of nodes locally using weighting with shape features such as distance to surface, surface curvature, skeletonization,

3. optimize the regularity of node distances and

4. generate the mesh.

For fast meshing in 3D with a dense mesh at the surface, we fix the surface nodes before the node reduction in step 2 and leave out the optimization in step 3. The original algorithm is restricted to objects consisting of only one material. Our extension to multiple breast tissues applies individual meshing steps for each tissue with fixed nodes at the tissue interfaces.

3.4 Material models and incompressibility

For every tissue type a material model has to be defined, which describes the behavior of that material under load. Many different material models for breast tissues have been proposed in literature.[10, 11, 17–20] The models differ not only in the mathematical expression of the material model, *i.e.* the stress–strain relationship, but also in the actual material parameters, *i.e.* the hardness of the tissues. The proposed stress-strain relationships are linear elastic, hyperelastic or exponential. In a previous experiment the resulting forces needed for a realistic compression of the proposed materials were examined. The limits on the compression force were in most cases not realistic.[7] Only the material model described by Bakic[19] resulted in a plausible range. All authors assume the soft breast tissue is an incompressible material as it consists mainly of water, *i.e.* an applied deformation results only in a shape change not a change of the volume.

The used model here can be applied with all mentioned types of stress-strain relationships and approximates the incompressibility with the typical FEM solution using a Poisson's ratio near 0.5.

3.5 Deformation as plate compression

To mimic clinically applied breast compression, the deformation is formulated as a contact problem between the mesh of the software breast model and two compression plates.

The compression plates are modeled as rectangular plates with the material properties of plexiglas. They are also meshed using the above described meshing method. Additionally, so-called contact elements are defined between the surface nodes of the compression plates and the breast mesh, which prevent mutual penetration and transfer the displacement of the compression plates to the breast surface.

The movement of the surface nodes of the plates and the breast model which would be near the chest wall are restricted in the direction towards the body, so that the breast model can just spread out away from the chest wall and in the directions perpendicular to the compression. The compression is defined as the percentage of the diameter change of the breast model in the compression direction and realized as the displacement of both compression plates towards the center of the breast model.
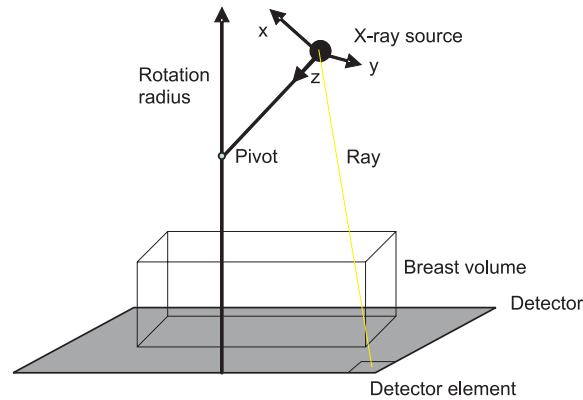
Figure 2. Geometry of the digital breast tomosynthesis system. The following parameters can be set: source and pivot position, position of the volume, discretization of the detector (number of rays), and interpolation points within the volume.

3.6 Reconstruction of the volume image of the deformed model

To simulate tomosynthesis projections, the volume image of the deformed anthropomorphic model was generated from the FEM results. The image is generated using the displacement information of the FEM model's nodes after the simulation and the gray value information of the original anthropomorphic model.

For a sufficient number of points within each finite element the actual displacement is calculated, using the node displacements and the shape functions of the elements. This displacement added to the undeformed position is equal to the deformed position. The voxel in the original breast, containing the undeformed point position, is calculated and its gray value is employed to interpolate the gray value of the corresponding voxel at the deformed position in the new volume. The gray values in the deformed phantom images are assigned to the nearest look-up table values by a nearest neighbor interpolation.

For a resulting image of good quality, the use of the inverse function of the transformation is usually recommended for interpolation. However, the inverse of the deformation of a finite element is not available. Therefore a sufficient number of points within the elements is needed to avoid voxels without gray value information. These voxel gaps depend strongly on the number of voxels per finite element and the amount of applied deformation.

4. SIMULATION OF TOMOSYNTHESIS PROJECTIONS AND RECONSTRUCTION OF TOMOSYNTHESIS VOLUMES

The x-ray source is simplified to be a point source emitting monoenergetic radiation without scatter. The projected values are then calculated as:

$$P(\vec{x}) = e^{\Sigma_i \mu_i dr} \tag{3}$$

where P is the projection image, $\vec{x}$ is the 2D pixel position in the projection, i is the control variable in the corresponding ray, μ_i the attenuation coefficient of the current voxel and dr is the discrete longitudinal sample width of the ray. This simplified model of x-rays is implemented as modular function so that it can be easily replaced by a more complex model.

We modeled a perspective projection with the point source in the focal point and the detector in the projection plane. The geometry of the projection can be defined arbitrarily to allow simulation of different setups for tomosynthesis. The geometry is given in Fig. 2.

The projection algorithm differs from the usually applied projection by matrix multiplication and may be better described as a 'ray tracing' approach. Thus the pixel positions of the detector and the rays per pixel can be fixed at the initial definition of the geometry, so that the values of the pixels do not have to be interpolated
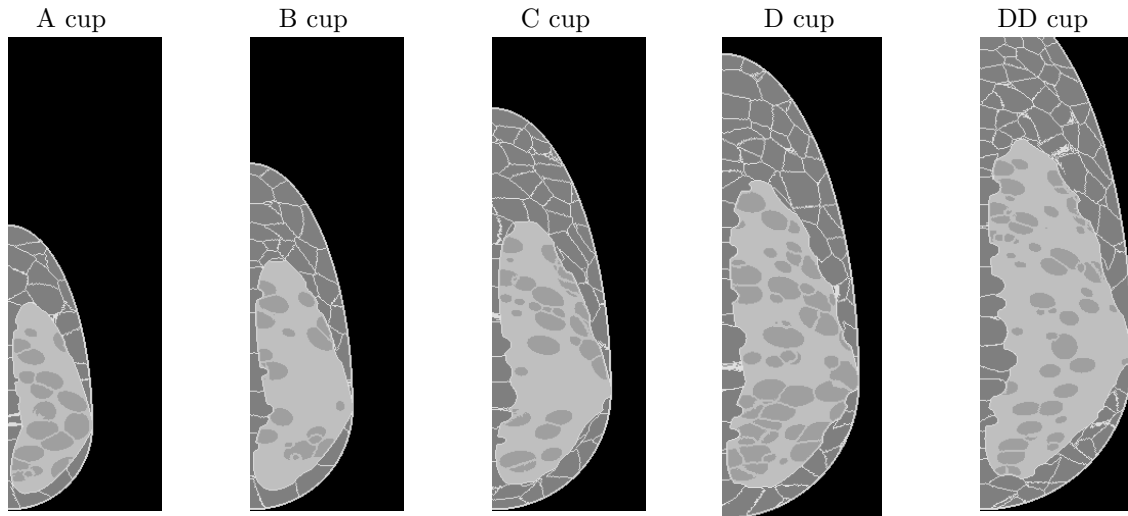
Figure 3. Cross-sections through five anthropomorphic breast phantoms. The breast phantoms have volumes corresponding to bra cup sizes A, B, C, D, and DD (as indicated in the figures).

(inverse formulation). Also the discretization level of rays can be defined to control the number of interpolation points per ray directly. The absorption coefficients at discrete ray points are interpolated from the image volume using a linear interpolation.

The projection simulation starts by defining 3D-vectors $\vec{x}$ from the source to the detector pixels in a Cartesian coordinate system with the origin defined at the source. These rays $\{\vec{x}\}$ are converted into $\{\vec{s}\}$ in the corresponding spherical coordinate system. As a result, the rays can be described simply by the pair of angles θ, ϕ and a line of linearly increasing radii. The radii r of the rays are discretized in steps of $dr < 0.5dp$, where dp is the voxel length, to follow Shannon's law for the interpolation. After that the actual projection is simple; the sampling points for the summation are given by all combinations of $\vec{s} = (\theta, \phi, r)^T$ inside the volume. The $\{\vec{s}\}$ are converted back to Cartesian coordinates giving a vector field $\{\vec{x'}\}$ which is used to interpolate the absorption values. The resulting gray values are calculated using the absorption coefficients μ per ray.

To carry out the projection of the deformed anthropomorphic phantom, appropriate linear x-ray attenuation coefficients μ are assigned to the corresponding tissue structures according to their look-up table values. The generated projections are converted into DICOM format to provide compatibility with any clinically applied reconstruction algorithm.

4.1 Reconstruction of tomosynthesis volumes

Tomographic reconstruction is performed using a filtered back-projection algorithm. This algorithm has been used in a clinical study of multimodality breast imaging at the Hospital of the University of Pennsylvania.[21]

5. RESULTS

5.1 Generated database of software phantoms

To cover variations in breast anatomy, we generated five phantoms of different volumes, corresponding to the available bra cup sizes: A (250 ml), B (450 ml), C (700 ml), D (950 ml) and DD (1500 ml), based on published values[22] (rounded). All phantoms have approximately 30 % glandularity and roughly between 350 to 550 compartments. Fig. 3 shows the central slices of the five phantoms. The tissue distribution is visualized using the look-up table of unique gray values assigned to each tissue type.
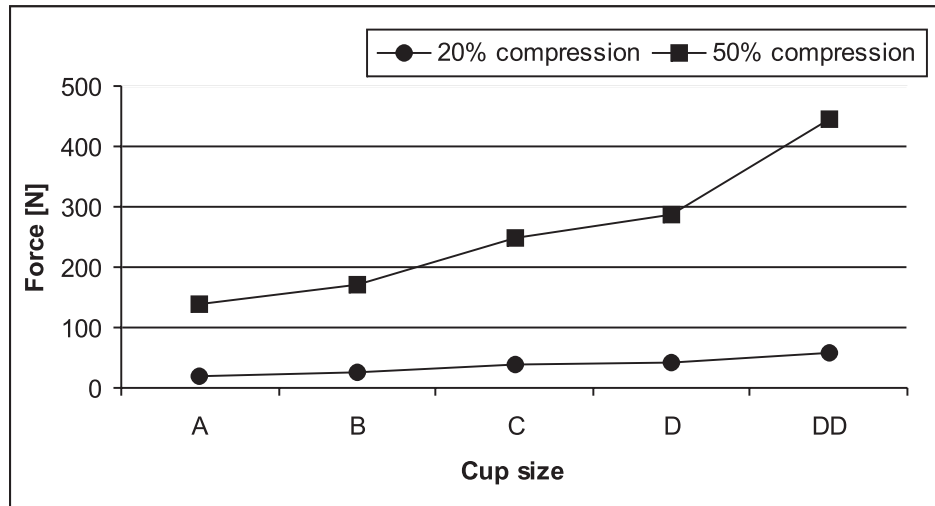
Figure 4. Simulated compression force in [N] as a function of breast cup size. The shown compression forces result in 20 % and 50 % reduced breast thicknesses.

5.2 Finite element simulation

For each phantom an individual finite element mesh was generated. On average the finite element meshes consisted of 5827 tetrahedrons. Each phantom was subjected to 20 and 50 % reduction in uncompressed thickness, mimicking the range of compression commonly used in tomosynthesis and mammography. For this example the breast tissues were modeled as homogenous, isotropic, Neo-Hookean, near incompressible materials (Poisson's ratio $\nu = 0.475$).

We used tissue elasticity corresponding to adipose tissues (Young's modulus E = 48.6 kPa [19]), which gave the most realistic compression forces in previous experiments (see 3.4). For the large deformation and to support the incompressibility constraint the linear material model

$$\sigma(\varepsilon) = E\varepsilon \tag{4}$$

with σ stress, E Young's modulus and ε strain, was approximated by the hyperelastic Neo-Hookean relationship

$$\sigma(\varepsilon) = \alpha((1+\varepsilon)^2 + (1+\varepsilon)^{-4}) \tag{5}$$

with the material constant $\alpha = 10.1$ kPa for the Neo-Hookean model.

To test the compression of the software phantoms quantitatively, the overall forces necessary for compression to 20 and 50 % were retrieved from the FEM results. Fig. 4 shows the resulting compression forces of the simulations ranging from the smallest (cup size A) to the largest (cup size DD) software phantom.

The resulting compression forces ranged between 17 N and 448 N. For the smaller breast volumes, up to cup size C, the forces fit well with the range of compression forces measured during clinical mammography (between 49 and 186 N [23]). For the larger volumes the 50 % compression resulted in higher forces. We plan to clarify this issue further by measuring clinical forces in women with different cup sizes, we hypothesize that large breasts are subjected to smaller percentage of compression. Nevertheless, the shape of the compressed breast phantom and the outline of the phantom in the tomosynthesis projections is realistic.

5.3 Simulated tomosynthesis projections

The geometry of the perspective projection resembles the tomosynthesis setup currently used in our clinical study (Senograph DS, GE, Milwaukee, WI). The digital detector has dimensions of 230.4 mm x 192 mm, with (0.1 mm)^2 sized detector elements.
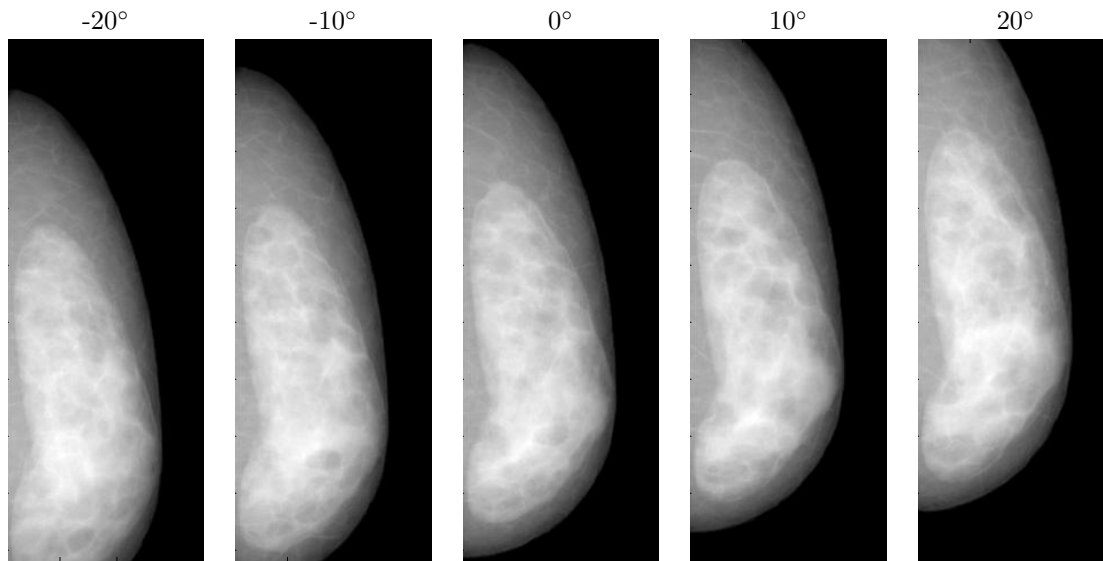
| -20° | -10° | 0° | 10° | 20° |

Figure 5. Simulated tomosynthesis projection images of an anthropomorphic breast phantom acquired at five different tube angles (as indicated in the figures). The breast phantom has a volume corresponding to bra cup size C and was subjected to a compression resulting in a 20 % reduced breast thickness.

The linear x-ray attenuation coefficients are set to $\mu_1 = 0.456\,\text{cm}^{-1}$ for adipose tissue and $\mu_2 = 0.802\,\text{cm}^{-1}$ for glandular and connective tissue and skin at 20 keV.[24] Fig. 5 shows projections through the deformed phantom (20 %) of cup size C. The projections look quite realistic, even though scatter is not included and only monoenergetic x-rays are assumed.

5.4 Simulated tomosynthesis reconstructions

The tomosynthesis reconstructions were performed by mimicking the setup of the actual tomosynthesis machine. The total range of projection angles is 20°, 30° or 40°, discretized to 7, 11, 13 or 15 equiangular steps. Fig. 6 shows slices through different reconstructed tomosynthesis volumes. The combination of 40° range and 30 steps was chosen to simulate a non-clinical setup.

The first four images show the same phantom reconstructed with an increasing number of projections. As expected, increasing the number of projections resulted in increased contrast and fewer artifacts. The last image shows the 40°/15 reconstruction of the same phantom but with 50 % deformation. Due to the current simplifications of the projection simulation the tissue contrast is not enhanced by higher compression. The image only shows the 3D effects of the deformation modeling, as the compartment are stretched to larger diameters and also a few different structures are visible than in the corresponding 20 % compression slice.

6. DISCUSSION AND CONCLUSION

A previously developed software phantom for x-ray mammography simulation has been extended to include a finite element model of realistic mammographic breast deformation, and to simulate tomosynthetic breast image acquisition.

The proposed schema for simulation of tomosynthesis projections of a software breast phantom can generate a wide variety of synthetic breast images. The size and texture of the breast to be simulated can be varied, as well as the amount of applied compression, and the geometry and parameters of the tomosynthesis setup. This simulation framework can facilitate evaluation of image processing algorithms. Examples of phantom application may include testing radiologist's performance in mammography and tomosynthesis by performing observer studies with various realistic tissue backgrounds; or testing the performance of registration algorithms by registering
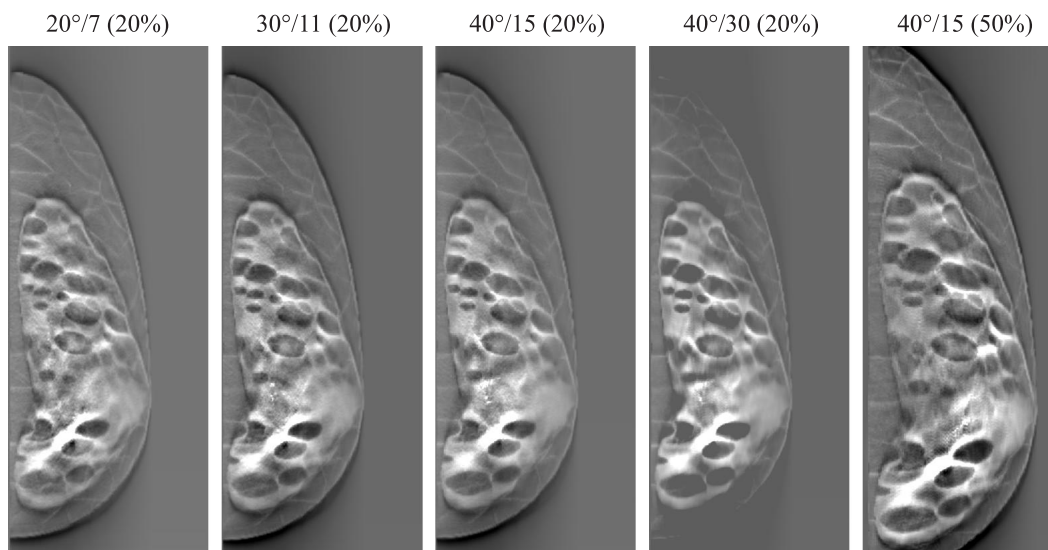
Figure 6. Simulated reconstructed tomosynthesis images of an anthropomorphic breast phantom for five tomosynthesis acquisition geometries. The acquisition geometries differ by the range of projection angles and number of projection images (indicated in the figure as range/number (compression)). The breast phantom has a volume corresponding to bra cup size C and was subjected to a compression resulting in a 20 % or 50 % reduced breast thickness.

simulated images with different amounts of compression. The realism of the reconstructed tomosynthesis projections and volumes will be further evaluated by comparison of the texture of the simulated images to clinical data. Future extensions to the described simulation approach will include analysis of different material models for the finite element model, different models for the interaction of skin and the compression plates, introduction of multi-energetic x-ray spectra, and realistic noise models.

REFERENCES

1. L. T. Niklason *et al.*, "Digital tomosynthesis in breast imaging," *Radiol.* **205**, pp. 399–409, 1997.
2. E. A. Rafferty *et al.*, "Tomosynthesis: New weapon in breast cancer fight," *Decis. in Imag. Econom* **17**, 2004.
3. P. R. Bakic *et al.*, "Mammogram synthesis using a 3D simulation. I. breast tissue model and image acquisition simulation," *Med. Phys.* **29**(9), pp. 2131–9, 2002.
4. F. Richard *et al.*, "Mammogram registration: a phantom-based evaluation of mammographic compression effects," *IEEE TMI* **25**(1), pp. 188–97, 2006.
5. R. A. Hunt *et al.*, "Calculation of the properties of digital mammograms using a computer simulation," *Radiat. Prot. Dosim.* **114**(1-3), pp. 397–400, 2005.
6. D. W. Mundy *et al.*, "Radiation binary targeted therapy for HER-2 positive breast cancers: assumptions, theoretical assessment and future directions," *PMB* **51**, pp. 1377–91, 2006.
7. N. V. Ruiter *et al.*, "Model-based registration of X-ray mammograms and MR images of the female breast," *IEEE Trans. Nucl. Sc.* **53**, 2006.
8. P. R. Bakic *et al.*, "Mammogram synthesis using a 3D simulation. II. evaluation of synthetic mammogram texture," *Med. Phys.* **29**(9), pp. 2140–51, 2002.
9. C. Zhang *et al.*, "Development of an antropomorphic breast software phantom based on region growing algorithm," in *SPIE Medical Imaging 2008: Visualization, Image-guided Procedures, and Modeling*, **6918**, 2008.
10. F. S. Azar, *A Deformable Finite Element Model of the Breast for Predicting Mechanical Deformations under External Perturbations.* PhD thesis, University of Pennsylvania, USA, 2001.

11. A. Samani *et al.*, "Biomechanical 3–D Finite Element Modeling of the Human Breast for MR/X–ray using MRI Data," *IEEE Transactions on Medical Imaging* **20**(4), 2001.

12. C. Tanner *et al.*, "Comparison of biomechanical breast models: A case study," in *Proceedings of SPIE Medical Imaging, Image Processing*, **4683**, 2002.

13. P. Pathmanathan *et al.*, "Predicting tumour location by simulating large deformations of the breast using a 3D finite element model and nonlinear elasticity," *Lecture Notes in Computer Science* **3217**, pp. 217–24, 2004.

14. O. C. Zienkiewicz *et al.*, *The Finite Elemente Method – volume 1*, Butterworth Heinemann, 5 ed., 2000.

15. M. Kleiber, *Handbook of Computational Solid Mechanics: Survey and Comparision of Contemporary Methods*, Springer–Verlag, 1998.

16. P. O. Persson, *Mesh Generation for Implicit Geometries*. PhD thesis, Massachusetts Institute of Technology, USA, 2005.

17. P. S. Wellman, *Tactile Imaging*. PhD thesis, Havard University, USA, 1999.

18. T. A. Krouskop *et al.*, "Elastic moduli of breast and prostate tissues under compression," *Ultrasonic Imaging* **20**, 1998.

19. P. R. Bakic *et al.*, "An approach to using a generalized breast model to segment digital mammograms," in *Proceedings of 11th IEEE Symposium on Computer–Based Medical Systems*, 1998.

20. J. Lorenzen *et al.*, "MR elastography of the breast: Preliminary clinical results," *RoFo Fortschritte auf dem Gebiet der Röntgenstrahlen und der bildgebenden Verfahren* **174**(7), 2002.

21. S. C. Chen *et al.*, "Initial clinical experience with contrast-enhanced digital breast tomosynthesis," *Acad. Radiol.* **14**(2), pp. 229–38, 2007.

22. A. Ringberg *et al.*, "Of cup and bra size: Reply to a prospective study of breast size and premenopausal breast cancer incidence," *Intern. J. Canc.* **119**(9), 2006.

23. D. C. Sullivan *et al.*, "Measurement of force applied during mammography," *Radiol.* **181**(2), pp. 55–7, 1991.

24. P. C. Johns *et al.*, "X-ray characterization of normal and neoplastic breast tissues," *Phys. in Med. and Biol.* **32**, pp. 675–695, 1987.